

Compact Graph Representation of crystal structures using Point-wise Distance Distributions

Jonathan Balasingham,^{*} Viktor Zamaraev,[†] and Vitaliy Kurlin[‡]

University of Liverpool

Department of Computer Science

Ashton Building, Liverpool L69 3DR, United Kingdom

(Dated: February 8, 2023)

Use of graphs to represent crystal structures has become popular in recent years as they provide a natural translation from atoms and bonds to nodes and edges. Graphs capture structure, while remaining invariant to the symmetries that crystals display. Several works in property prediction, including those with state-of-the-art results, make use of the *Crystal Graph*. The present work offers a graph based on Point-wise Distance Distributions which retains symmetrical invariance, decreases computational load, and yields similar or better prediction accuracy on both experimental and simulated crystals.

I. INTRODUCTION

Determining the properties of crystals requires the employment of techniques such as Density Functional Theory (DFT) [1]. Unfortunately, applying these methods requires extensive domain knowledge and is computationally expensive. Furthermore, DFT calculations are known to introduce their own error due to the relaxation of constraints required to make the computations feasible [2]. These reasons have led to the application of machine learning algorithms as a substitute to decrease computation time and greatly (if not eliminate) the need for domain knowledge. In early works, machine learning algorithms like kernel regression [3], feed-forward neural networks [4] and ensemble methods [5] were used. While these methods showed potential, they were not methods made to work with structured data, such as the case with crystals and molecules. Graph Neural Networks (GNN) [6] directly addressed this concern by providing a straightforward way to encode the information for atoms and bonds in the nodes and edges of a graph. Representing a molecule with a GNN is evident, but crystals are more complex. Crystals can have arbitrary sizes and display their symmetries in a periodic way. One of the most prominent works to address this problem was the Crystal Graph Convolutional Neural Network (CGCNN) [7]. Along with a novel graph convolution layer that incorporated node and edge information, they also proposed a graph representation of a crystal known as a crystal graph. From this point, the crystal graph representation has been used in many other works where GNNs have been utilized for materials property prediction [8–13] including the state-of-the-art model (for Materials Project data), ALIGNN [14]. Models that base themselves off of CGCNN attempt to gain improvement by incorporating three-body interactions between atoms [15], changing

edges to be defined as bonds by using a cutoff radius [16], or using specialized attention masks to add geometric information [17]. Here, we wish to propose a new way to represent crystals with a graph. We will provide a graph representation of a crystal that is invariant to symmetry relations and unit cell choice. To do this, we employ the ideas behind the Point-wise Distance Distribution (PDD) [18][19] which take advantage of atoms within the unit cell that display identical behavior. Additionally, we will introduce two versions of this graph that can be selected based upon the property being predicted. By doing so, we can prioritize either compositional or structural information to improve prediction accuracy. The model will be applied on two distinct datasets: the T2 [20] simulated crystals and the Materials Project crystals [21]. We will focus on property prediction of lattice [22][23], formation [24], and band gap energy [25].

Since it is our aim to improve upon the crystal graph, it is important to understand how this graph is created. The graph can be said to be parameterized by two values: k , the number of nearest neighbors, and r , the cutoff radius. If we consider the atoms within a given crystal's unit cell, then for each member we find the k nearest neighbors by euclidean distance that are within r angstroms of that atom. The convolutional layer developed by the authors of CGCNN can appropriately weigh distant atoms accordingly, so their interactions are weakened. As such, when testing the crystal graph we use an adequately large r to have k neighbors for each node. Once the neighbors of an atom are found, an edge is established between the node representing the atom and each of its neighbors. If the neighbor resides outside of the original cell, the atom within the unit cell which corresponds to that atom under translation is used instead. The result is a graph with the number of nodes equal to the number of atoms within the unit cell and the number of directed multi-edges equal to k times the number of nodes. When we refer to atoms within the unit cell, we refer specifically to the unit cell as defined by the data from which the crystal came. This means that the graph produced will be different for different choices of unit cell. Additionally, if the unit cell defined by the data is

^{*} jbalasin@liverpool.ac.uk

[†] Viktor.Zamaraev@liverpool.ac.uk

[‡] Vitaliy.Kurlin@liverpool.ac.uk

arbitrarily large, then the graph will increase in size accordingly. The use of larger unit cells, called supercells, has its own applications [26] and coming across data with such transformations is possible. The onus of using the smallest possible cell is placed on the cleanliness of the data or otherwise, must be achieved by user intervention.

II. METHODOLOGY

We first define a PDD, upon which our graph is built. A crystal structure can be defined in terms of a periodic point set [27].

Definition 1 For a set of n basis vectors $\mathbf{v}_1 \dots \mathbf{v}_n \in \mathbb{R}^n$, the lattice Λ is formed by the integer linear combinations of these basis vectors $\{\sum_{i=1}^n c_i \mathbf{v}_i | c_i \in \mathbb{Z}\}$. When $c_i \in [0, 1)$ we obtain the unit cell U .

Definition 2 For a unit cell U in the lattice $\Lambda \subset \mathbb{R}^n$, the motif M is a finite subset of U .

Definition 3 A periodic point set P of lattice Λ and motif M is defined by the Minkowski sum of M and Λ , $\{\lambda + p : \lambda \in \Lambda, p \in M\}$.

As such, a given lattice has an infinite number of valid unit cells. The PDD of a periodic point set P is a matrix whose rows consist of the distance to each of the k nearest neighbors in P for each point contained within U . The number of nearest neighbors k can be considered a parameter to be selected. For every row in this matrix, a weight w_i is assigned equal to $\frac{1}{m}$ such that $\sum_{i=1}^m w_i = 1$ where m is the number of motif points within U . If any row is found to have duplicates within the matrix, these rows are collapsed into a single row and their respective weights are added. It is also common to allow for some tolerance at which rows can be collapsed without necessarily having a distance of exactly zero between them. Here duplicates are determined by finding the distance between two rows using the L_{inf} norm, but any valid metric can be used. Finally, the rows of the matrix are lexicographically ordered. The PDD has distinct qualities that we take advantage of when converting to a graph:

1. No matter the choice of unit cell, the PDD will be the same provided that the collapse tolerance and parameter k are the same [18].
2. The number of atoms in the PDD will be equal or less than the number of atoms in the unit cell. This allows us to compress the resulting representation.

Here we will also introduce the concept of the *constrained* PDD. This PDD has the additional condition that rows in the matrix which are collapsed must have the same atom species.

For example, consider Lutetium-Silicon (shown in Figure 1). The unit cell selected contains four atoms. If we

consider the 2 nearest neighbors, the PDD matrix of this periodic set S before collapsing can be written as,

$$PDD(S; k) = \begin{pmatrix} 0.25 & 2.481 & 2.481 \\ 0.25 & 2.481 & 2.481 \\ 0.25 & 2.881 & 2.881 \\ 0.25 & 2.881 & 2.881 \end{pmatrix}$$

where the first column of this matrix represents the weight for each row (atom); the second is the distance to the nearest neighbor and the third, the distance to the second nearest neighbor. The first two rows are identical, as are the final two. Because of this, we can collapse each set into a single row producing

$$PDD(S; k) = \begin{pmatrix} 0.5 & 2.481 & 2.481 \\ 0.5 & 2.881 & 2.881 \end{pmatrix}$$

This is the finalized PDD. If the unit cell is expanded, this collapsing will continue to yield the same result as the proportion of each atom (and the distance to their neighbors) will remain the same.

A. Point-wise Distance Distribution Graph

The weighted graph representation created here is derived directly from the PDD matrix. For a given PDD of size $m \times k$, the number of nodes within the graph will be equivalent to m , the number of rows in the PDD. For each of the k nearest neighbors contained in the PDD we establish an edge between that row's corresponding node and the node to which it corresponds before translation is applied. The weight of this edge is equivalent to the euclidean distance between the two atoms. The resulting directed multi-graph will have m nodes and mk outgoing edges. As a multi-graph, there can be multiple edges (with direction) between any two nodes. The graph can also include self-loops, a directed edge from a node to itself. The aforementioned tolerance (henceforth referred to as the *collapse tolerance*) will be treated as a hyper-parameter to be selected. Each of the nodes in the formed graph will carry the weight from the PDD. Note, we use a normalized weight per graph such that for any given graph the sum of all weights is equal to one, but this could be substituted with the raw count of the number of occurrences of that row within the PDD. If this is done, the PDD graph will mimic the behavior of the crystal graph, with the only difference being the size of the graph which will have potentially fewer vertices and edges. An example of how the crystal graph compares to this PDD graph can be seen in Figure 1 for Lutetium-Silicon.

B. Model

To make use of this representation, we must modify the traditional graph neural network framework to take

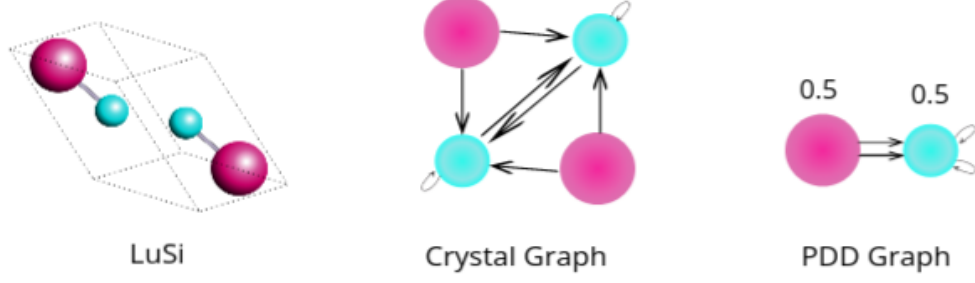


FIG. 1. The transformation from crystal structure of LuSi to the crystal graph and PDD graph with $k = 2$ nearest neighbors and a collapse tolerance of 10^{-6} . Lutetium is colored in magenta while Silicon is colored in teal.

advantage of the weighted vertices. We must make these changes to two specific operations: normalization and graph readout. The computations we propose here can be applied in a general setting for GNNs which take advantage of a number of different mechanisms including convolution, attention, or message-passing layers. For consistency, we will make use of CGCNN which was proposed in the original paper from which the crystal graph was created.

A single convolution from CGCNN can be defined by the equations [7],

$$\mathbf{v}_i^{(t+1)} = \mathbf{v}_i^{(t)} + \sum_{j,k} \sigma(\mathbf{z}_{(i,j)_k}^{(t)} \mathbf{W}_f^{(t)} + \mathbf{b}_f^{(t)}) \odot g(\mathbf{z}_{(i,j)_k}^{(t)} \mathbf{W}_s^{(t)} + \mathbf{b}_s^{(t)}) \quad (1)$$

where

$$\mathbf{z}_{(i,j)_k}^{(t)} = \mathbf{v}_i^{(t)} \oplus \mathbf{v}_j^{(t)} \oplus \mathbf{u}_{(i,j)_k}$$

and $\mathbf{v}_i^{(t)}$ is the embedding of the i^{th} node after t convolutions, $\mathbf{u}_{(i,j)_k}$ are the edge features of k^{th} edge between nodes i and j and $\mathbf{W}_f^{(t)}, \mathbf{W}_s^{(t)}$ and $\mathbf{b}_f^{(t)}, \mathbf{b}_s^{(t)}$ are the learned weight and bias matrices, respectively. The operator \oplus refers to concatenation and \odot , to element-wise multiplication.

1. Normalization

Normalization is a data scaling technique commonly used to increase model stability and improve training efficiency [28]. Two commonly used types are batch normalization [29] and layer normalization [30]; each of which operate on different dimensions of the input. Layer normalization scales features with respect to one another, within a single sample. In batch normalization, normalization is done over multiple samples for a single feature.

In GNNs the result of layer normalization on nodes is not dependent on the number of nodes in any given

graph, since the computation operates on the features of just that node. This cannot be said of batch normalization. In a single batch it is necessary to operate on multiple graphs at once. These graphs have no requirement to consist of the same number of nodes. Because of this, it is possible that a single graph can be over-represented in the mean or variance computed during normalization. While it is usually not a problem in many GNN applications, graphs used to represent crystals which depend on the unit cell can fall victim to this. One could arbitrarily scale a crystal's unit cell size, or select different basis vectors and predictions for the model trained on this altered data would be different despite using the same underlying data and hyper-parameters. Use of the PDD graph alleviates the concerns over unit cell selection by the use of weights within the batch normalization. The weighted batch normalization for a batch b containing graphs G_1, \dots, G_n with a respective number of nodes g_1, \dots, g_n can be computed using

$$\mu_b = \frac{\sum_{j=1}^n \sum_{i=1}^{g_j} w_{ij} \mathbf{v}_{ij}}{B} \quad (2)$$

$$\sigma_b^2 = \frac{\sum_{j=1}^n \sum_{i=1}^{g_j} w_{ij} (\mathbf{v}_{ij} - \mu_b)^2}{B} \quad (3)$$

$$N(\mathbf{v}) = \frac{\mathbf{v} - \mu_b}{\sigma_b} \quad (4)$$

where $B = \sum_{j=1}^n \sum_{i=1}^{g_j} w_{ij}$, \mathbf{v}_{ij} is the i^{th} vertex embedding in the j^{th} graph, and w_{ij} is the weight of the i^{th} node in the j^{th} graph. Eq. 3 and Eq. 4 are used to compute the weighted mean and weighted biased variance of the batch respectively. Finally, Eq. 5 provides the formula for normalizing a given sample or node \mathbf{v} from batch b .

2. Graph Readout

The readout or pooling layer of a GNN is used to condense the information contained within the individual node embeddings into a single vector representative of the whole graph. This vector is commonly passed to a multi-layer perceptron for a prediction to be made. While there are many options for a pooling layer, they all must retain the property of permutational invariance (order of the node embeddings does not matter). Some of the most common graph readouts are maximum and mean pooling and normalized sum. In the former case, no adjustments need to be made as the maximum of each feature within the embedding does not depend on the number of vertices. For the latter two, this is not true. For mean pooling, we must use the weighted average of the node embeddings defined by

$$\mathbf{v}_c = \sum_i w_i \mathbf{v}_i \quad (5)$$

For the normalized sum, we can again use Eq. 5 and then apply layer normalization on the result.

III. EXPERIMENTS

A. Datasets

The Materials Project dataset contains 36,678 crystal structures with a wide range of compositions, unit cell types, and symmetries. The T2 dataset is much smaller at 5,687 samples, all with the same underlying molecule. As such, obtaining good performance across both sets of data requires the model to learn the complex relation between atomic composition, structure and the desired property when either composition or structure can act as the primary differentiator. Furthermore, the datasets display significant differences in unit cell content size (and thus resulting graph sizes). Figure 2 shows the distribution of the number of atoms within the unit cell in each dataset. The mean number of atoms in the unit cell for the T2 crystals is just over 361, while the Materials Project data has a mean of just 25.84.

B. Impact of Collapse Tolerance on Compression

In Figure 3 the distribution of the number of nodes in the (unconstrained) PDD graph representation is displayed using smoothing from kernel density estimation for the Materials Project data when considering the 12 nearest neighbors (the same as the paper which proposed CGCNN). Figure 4 provides the same estimation for the T2 dataset, but for the 16 nearest neighbors. This increase in k is due to the increased number of atoms in the unit cell, while also considering hardware limitations.

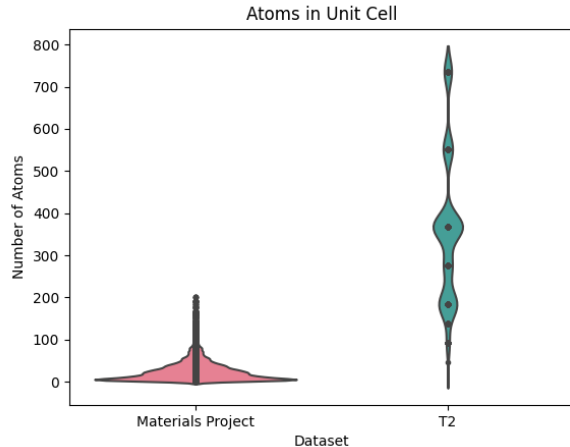


FIG. 2. Distribution of the number of atoms within the unit cell for the Materials Project and T2 datasets.

The plot for 'No Collapse' represents the number of nodes that would be in the original crystal graph. The decrease in the number of nodes for T2 and the Materials Project is shown in Table I. The crystals within the Materials Project experience relatively small amounts of compression on average between 10^{-8} and 10^{-4} decreasing from 10.61 to 10.21 and then finally to 9.09. Further inspection of this result shows that these drops in the average come from a small subset (roughly 2,500) of the crystals which experience significant drops in graph size. The T2 crystals, on the other hand, experience consistent drops in graph size (from 361) with mean values of 271.84, 110.87 and 86.9 for tolerances of 10^{-8} , 10^{-6} and 10^{-4} respectively.

C. Impact of Collapse Tolerance on accuracy

Here we will look at how collapse tolerance effects the accuracy of model predictions. We have chosen to use 80/10/10 splits for the training, test, and validation sets

TABLE I. Average reduction in nodes compared to the crystal graph at various collapse tolerances for the T2 and Materials Project (MP) datasets.

Dataset	Tolerance	Nodes	Compression ^a
T2	N/A	361.3	100.0%
T2	10^{-8}	271.8	78.5%
T2	10^{-6}	110.87	30.5%
T2	10^{-4}	86.9	24.4%
MP	N/A	25.8	100.0%
MP	10^{-8}	10.6	44.1%
MP	10^{-6}	10.2	42.8%
MP	10^{-4}	9.1	38.9%

^a Average percent of the number of nodes in the Crystal Graph

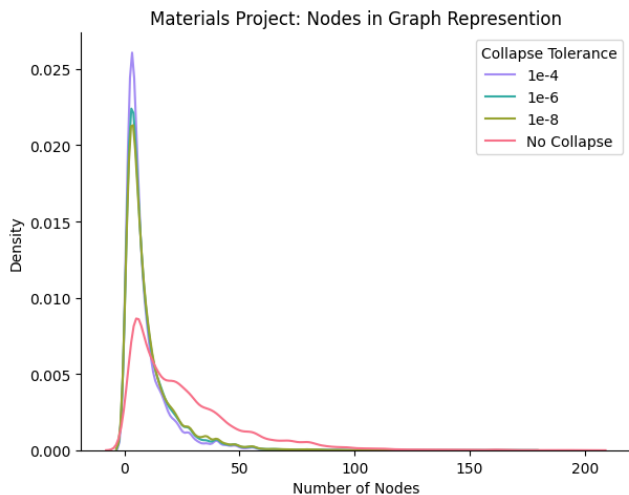


FIG. 3. Kernel Density Estimation of the distribution of the number of nodes within the graph representation for the Materials Project dataset at varying collapse tolerances. 'No Collapse' would correspond to the size of the crystal graph.

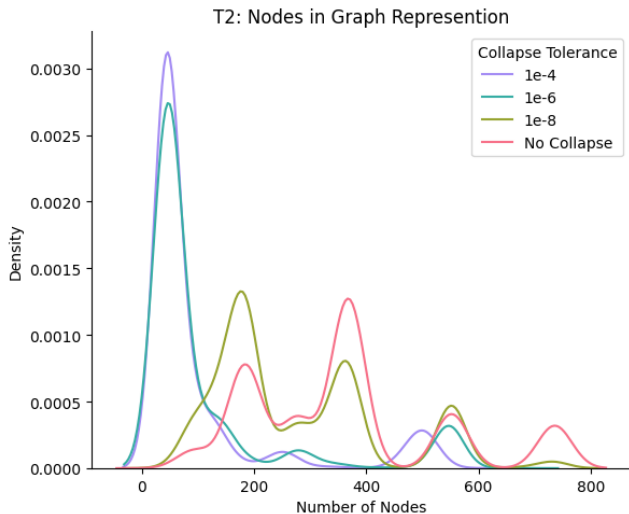


FIG. 4. Kernel Density Estimation of the distribution of the number of nodes within the graph representation for the T2 dataset at varying collapse tolerances. 'No Collapse' would correspond to the size of the crystal graph.

respectively. The collapse tolerance for the PDD will again vary between $(0, 10^{-4}]$. Table II shows the resulting mean absolute errors (MAE) across each of the collapse tolerances. Results for the PDD graph that do not indicate a collapse tolerance do not collapse atoms but do utilize weights and the weighted batch normalization described in the previous section. The results for band gap energy are stable across the various tolerances even performing better than the crystal graph at higher tolerances, however this is not true for formation energy. The MAE for the model with tolerance between 10^{-8} and 10^{-4} is significantly worse. The reason for this in-

crease in loss can be attributed to the collapsing of rows which correspond to two different atom types. A simple example of this can be seen when there are two atoms in the unit cell with different types. Each atom can easily display the same distances to their k -nearest neighbors, resulting in collapse and significant loss of information. The uncollapsed version, which took advantage of our weighted batch normalization and weighted readout did improve upon the crystal graph result. This version, limits individual crystals from shifting the mean and variance of the batch normalization in accordance with their size, but is not invariant to unit cell selection due to the lack of collapsing. The results in Table II can be referred to as making use of the *unconstrained* version of compression. If we use the constrained PDD to build our graph, we can obtain the results in Table III using *constrained* compression.

Using this technique, the results for formation energy improve significantly. Across all collapse tolerances, we achieve an equal or more accurate result than the original crystal graph. This accuracy is obtained while shrinking the graph representation to between 43.7% and 48.8% of the original size. The results for band gap energy change only slightly, but maintain their improvement upon the accuracy of the crystal graph.

The variation in the results between the unconstrained and constrained compression exposes an interesting difference between formation and band gap energy. The ability to collapse away some species of atoms within the crystal while maintaining prediction accuracy indicates that band gap energy is more a product of the geometrical structure rather than the crystal's composition. The deterioration of the results for formation energy indicates the opposite: the composition is more crucial than the geometrical structure of the crystal.

Table IV shows the results for the analogous experiment conducted on the T2 dataset for prediction of lattice energy using unconstrained compression. Compression actually helps the accuracy of predictions for this

TABLE II. Prediction mean-absolute-error on formation energy (FE) and band gap (BG) energy for crystal in the Materials Project data by collapse tolerance for and PDD graph compared to the crystal graph at $k = 12$ nearest neighbors.

Graph	Tolerance	Property	MAE	Compression ^a
CG	N/A	FE	0.051	100.0%
PDD	N/A	FE	0.047	100.0%
PDD	10^{-8}	FE	0.07	44.1%
PDD	10^{-6}	FE	0.071	42.8%
PDD	10^{-4}	FE	0.072	38.9%
CG	N/A	BG	0.338	100.0%
PDD	N/A	BG	0.329	100.0%
PDD	10^{-8}	BG	0.327	44.1%
PDD	10^{-6}	BG	0.317	42.8%
PDD	10^{-4}	BG	0.323	38.9%

^a Average percent of the number of nodes in the Crystal Graph

dataset. The reason behind this cannot be determined for certain, but due to the small size of the dataset, the compression can prevent overfitting from occurring by removing small differences in structure. This allows the model to better generalize and thus, produce better results on the test set. We saw how compression can negatively effect properties that depend heavily on compositional information. This dataset is homogeneous in its composition; thus compression does not cause the accuracy of predictions to suffer. We are able to shrink the crystals to just 24.4% of the original size of the crystal graph and reduce MAE by 0.091.

D. Selection of k -Nearest Neighbors

The choice of k nearest neighbors from which to construct the graph has a heavy influence on performance for lattice energy. Even with aggressive compression at a collapse tolerance of 10^{-4} increasing k comes with sizeable reductions in MAE. For example, an increase from 16 to 18 can reduce MAE from 3.27 to 2.98. The increase in k is not without cost. Memory consumption is increased significantly, but due to the more compact nature of the PDD graph this does not become a problem until k reaches 25. The same cannot be said of the crystal graph, which requires intervention to run the model at such settings. This comes in the form of reducing the batch size, which reduces performance of the batch normalization (and thus, prediction accuracy) or through clearing data from the cache, greatly slowing down training.

Table V show the decrease in MAE as a result of increasing the k -nearest neighbors. With each increase in k , the number of the edges in the PDD graph increases proportionately with the number of nodes in the graph, assuming the number of collapses is the same. With a higher number of k , the additional distances in the PDD can prevent the collapsing of rows. We can see this is the case by looking at the number of nodes listed in table V.

TABLE III. Prediction mean-absolute-error on formation energy (FE) and band gap (BG) energy for crystal in the Materials Project data by collapse tolerance using constrained compression for the PDD graph compared to the crystal graph at $k = 12$ nearest neighbors.

Graph	Tolerance	Property	MAE	Compression ^a
CG	N/A	FE	0.051	100.0%
PDD	10^{-8}	FE	0.048	48.8%
PDD	10^{-6}	FE	0.049	47.5%
PDD	10^{-4}	FE	0.05	43.7%
CG	N/A	BG	0.338	100.0%
PDD	10^{-8}	BG	0.325	48.8%
PDD	10^{-6}	BG	0.326	47.5%
PDD	10^{-4}	BG	0.322	43.7%

^a Average percent of the number of nodes in the Crystal Graph

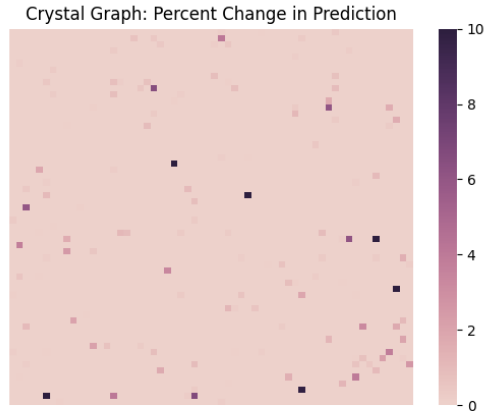


FIG. 5. Absolute Percent difference in prediction of formation energies for the test set using the crystal graph after altering samples in the training data to have supercells.

Despite the sharp increase in the number of neighbors, we are able to have significant improvements over the crystal graph with fewer nodes and edges in the graph representation.

E. Impact of Unit Cell choice

A valid unit cell U for a given crystal can be transformed by multiplying the original basis vectors ($\mathbf{a}, \mathbf{b}, \mathbf{c}$) by a transformation matrix \mathbf{P} where $P_{ij} \in \mathbb{Z}$

$$\begin{pmatrix} P_{11} & P_{12} & P_{13} \\ P_{21} & P_{22} & P_{23} \\ P_{31} & P_{32} & P_{33} \end{pmatrix}$$

such that $\det(\mathbf{P}) = 1$ to maintain cell volume and $\det(\mathbf{P}) > 1$ for a supercell [31].

In this experiment, these transformations are done to the unit cell to form a supercell for 2,000 of the crystals (roughly 7%) from the training set of the Materials Project data. A control run was done using the original

TABLE IV. Prediction mean-absolute-error on lattice energy for crystal in the T2 data by collapse tolerance for the PDD graph compared to the crystal graph at $k = 16$ nearest neighbors.

Graph	Tolerance	Property	MAE ^a	Compression ^b
CG	N/A	LE	3.358	100.0%
PDD	N/A	LE	3.314	100.0%
PDD	10^{-8}	LE	3.339	78.5%
PDD	10^{-6}	LE	3.353	30.5%
PDD	10^{-4}	LE	3.267	24.4%

^a MAE of the test set

^b Average percent of the number of nodes in the Crystal Graph

TABLE V. Prediction MAE on lattice energy for crystals in the T2 dataset by k , the number of nearest neighbors, at a collapse tolerance of 10^{-4} .

Graph	k	Nodes ^a	Edges ^b	MAE
CG	16	361	4,332	3.358
PDD	12	87	1,043	4.306
PDD	15	99	1,494	3.355
PDD	18	104	1,878	2.983
PDD	21	107	2,254	2.762

^a Average number of nodes across dataset

^b Average number of edges in multi-graph across dataset

data, then the unit cells were altered for a second run. We chose to use formation energy as the band gap energy data has very small values that can result in inflated percent change. A heatmap of the absolute percent change in prediction between the first and second run for the crystal graph is shown in Figure 5. On average the predictions changed by 4.36%, with the maximum change being over 135% compared to its original value. The overall test MAE increased slightly from 0.501 to 0.502. With the PDD graph, the resulting graph would be the exact same regardless of the transformation to the unit cell. Intuitively, this can be seen as the PDD keeps track of the proportion of a particular atom within the cell through its weights and eliminates atoms with the same behavior through collapsing rows in the PDD. This collapsing removes the dependence of our graph from the unit cell choice.

IV. CONCLUSION

The PDD graph is a compact graph representation for periodic crystals that is invariant to symmetry operations and choice of unit cell. We have shown this representation, in conjunction with weighted batch normalization and weighted readout, can maintain the accuracy of the crystal graph while reducing the number of nodes and edges significantly. We have also introduced the collapse tolerance as a hyper-parameter which can be tuned to increase or decrease compression of the graph in line with ones requirements. The choice of constrained or unconstrained compression can be used, dependent on the crystal property one is attempting to predict. The collapse tolerance also allows the graph to be stable to atomic perturbations or small errors in measurement that can occur at the atomic level. By having fewer nodes and edges in the representation, we can speed up training and prediction time, as well as reduce memory requirements. Furthermore, users can elect to use absolute totals as weights instead of the normalized weights from the original PDD, and the resulting graph will produce the exact results as the crystal graph with fewer nodes and edges. The components we have provided here are general and can be applied to any of the other models that make use of the crystal graph to reduce compute time and improve accuracy.

-
- [1] D. S. Sholl and J. A. Steckel, *Density functional theory: a practical introduction* (John Wiley & Sons, 2011).
 - [2] A. J. Cohen, P. Mori-Sánchez, and W. Yang, Challenges for density functional theory, *Chemical reviews* **112**, 289 (2012).
 - [3] B. A. Calfa and J. R. Kitchin, Property prediction of crystalline solids from composition and crystal structure, *AICChE Journal* **62**, 2605 (2016).
 - [4] W. Ye, C. Chen, Z. Wang, I.-H. Chu, and S. P. Ong, Deep neural networks for accurate predictions of crystal stability, *Nature communications* **9**, 3800 (2018).
 - [5] B. Olsthoorn, R. M. Geilhufe, S. S. Borysov, and A. V. Balatsky, Band gap prediction for large organic crystal structures with machine learning, *Advanced Quantum Technologies* **2**, 1900023 (2019).
 - [6] F. Scarselli, M. Gori, A. C. Tsoi, M. Hagenbuchner, and G. Monfardini, The graph neural network model, *IEEE transactions on neural networks* **20**, 61 (2008).
 - [7] T. Xie and J. C. Grossman, Crystal graph convolutional neural networks for an accurate and interpretable prediction of material properties, *Physical Review Letters* **120**, 145301 (2018).
 - [8] C. J. Court, B. Yildirim, A. Jain, and J. M. Cole, 3-D inorganic crystal structure generation and property prediction via representation learning, *Journal of chemical information and modeling* **60**, 4518 (2020).
 - [9] S.-Y. Louis, Y. Zhao, A. Nasiri, X. Wang, Y. Song, F. Liu, and J. Hu, Graph convolutional neural networks with global attention for improved materials property prediction, *Physical Chemistry Chemical Physics* **22**, 18141 (2020).
 - [10] J. Schmidt, L. Pettersson, C. Verdozzi, S. Botti, and M. A. Marques, Crystal graph attention networks for the prediction of stable materials, *Science Advances* **7**, eabi7948 (2021).
 - [11] S. Sanyal, J. Balachandran, N. Yadati, A. Kumar, P. Rajagopalan, S. Sanyal, and P. Talukdar, MT-CGCNN: Integrating crystal graph convolutional neural network with multitask learning for material property prediction (2018).
 - [12] S. S. Omee, S.-Y. Louis, N. Fu, L. Wei, S. Dey, R. Dong, Q. Li, and J. Hu, Scalable deeper graph neural networks for high-performance materials property prediction, *Patterns*, 100491 (2022).
 - [13] K. Das, B. Samanta, P. Goyal, S.-C. Lee, S. Bhattacharjee, and N. Ganguly, CrysXPP: An explainable property predictor for crystalline materials, *npj Computational Materials* **8**, 43 (2022).
 - [14] K. Choudhary and B. DeCost, Atomistic line graph neural network for improved materials property predictions, *npj Computational Materials* **7**, 10.1038/s41524-021-00650-1 (2021).

- [15] C. W. Park and C. Wolverton, Developing an improved crystal graph convolutional neural network framework for accelerated materials discovery, *Physical Review Materials* **4**, 063801 (2020).
- [16] C. Chen, W. Ye, Y. Zuo, C. Zheng, and S. P. Ong, Graph networks as a universal machine learning framework for molecules and crystals, *Chemistry of Materials* **31**, 3564 (2019).
- [17] J. Cheng, C. Zhang, and L. Dong, A geometric-information-enhanced crystal graph network for predicting properties of materials, *Communications Materials* **2**, 1 (2021).
- [18] D. Widdowson and V. Kurlin, Resolving the data ambiguity for periodic crystals, *Advances in Neural Information Processing Systems (Proceedings of NeurIPS 2022)* **35** (2022).
- [19] D. Widdowson, M. Mosca, A. Pulido, A. Cooper, and V. Kurlin, Average minimum distances of periodic point sets - fundamental invariants for mapping all periodic crystals, *MATCH Communications in Mathematical and in Computer Chemistry* **87**, 529 (2022).
- [20] A. Pulido, L. Chen, T. Kaczorowski, D. Holden, M. A. Little, S. Y. Chong, B. J. Slater, D. P. McMahon, B. Bonillo, C. J. Stackhouse, A. Stephenson, C. M. Kane, R. Clowes, T. Hasell, A. I. Cooper, and G. M. Day, Functional materials discovery using energy-structure-function maps, *Nature* **543**, 657 (2017).
- [21] A. Jain, S. P. Ong, G. Hautier, W. Chen, W. D. Richards, S. Dacek, S. Cholia, D. Gunter, D. Skinner, G. Ceder, and K. a. Persson, The Materials Project: A materials genome approach to accelerating materials innovation, *Applied Physics Letters Materials* **1**, 011002 (2013).
- [22] J. Yang, W. Hu, D. Usvyat, D. Matthews, M. Schütz, and G. K.-L. Chan, Theoretical chemistry. ab initio determination of the crystalline benzene lattice energy to sub-kilojoule/mole accuracy, *Science* **345**, 640 (2014).
- [23] G. Bogdanov, J. Bustos, V. Glebov, E. Oskolkov, J. P. Tillotson, and T. V. Timofeeva, Molecular and crystal structure, lattice energy and dft calculations of two 2'-(nitro-benzo-yloxy)aceto-phenone isomers, *Acta crystallographica. Section E, Crystallographic communications* **76**, 857 (2020).
- [24] A. A. Emery and C. Wolverton, High-throughput dft calculations of formation energy, stability and oxygen vacancy formation energy of abo3 perovskites, *Scientific Data* **4**, 170153 (2017).
- [25] J. P. Perdew, Density functional theory and the band gap problem, *International Journal of Quantum Chemistry* **28**, 497 (1985).
- [26] K. Okhotnikov, T. Charpentier, and S. Cadars, Supercell program: a combinatorial structure-generation approach for the local-level modeling of atomic substitutions and partial occupancies in crystals, *Journal of cheminformatics* **8**, 1 (2016).
- [27] P. Smith and V. Kurlin, A practical algorithm for degree-k voronoi domains of three-dimensional periodic point sets, in *Lecture Notes in Computer Science (Proceedings of ISVC)*, Vol. 13599 (2022).
- [28] J. Shao, K. Hu, C. Wang, X. Xue, and B. Raj, Is normalization indispensable for training deep neural network?, *Advances in Neural Information Processing Systems* **33**, 13434 (2020).
- [29] S. Ioffe and C. Szegedy, Batch normalization: Accelerating deep network training by reducing internal covariate shift (2015).
- [30] J. Lei Ba, J. R. Kiros, and G. E. Hinton, Layer normalization, *ArXiv e-prints*, arXiv (2016).
- [31] H. Arnold, Transformations of the coordinate system (unit-cell transformations), (2006).